Journal of Power Sources 189 (2009) 449–453

Contents lists available at ScienceDirect

Journal of Power Sources

journal homepage: www.elsevier.com/locate/jpowsour

Short communication

Thin nanostructured $LiMn_2O_4$ films by flame spray deposition and *in situ* annealing method

S.Y. Chew[a,b], T.J. Patey[a], O. Waser[c], S.H. Ng[a], R. Büchel[c], A. Tricoli[c], F. Krumeich[d], J. Wang[b], H.K. Liu[b], S.E. Pratsinis[c], P. Novák[a,*]

[a] *Electrochemistry Laboratory, Paul Scherrer Institut, CH-5232 Villigen PSI, Switzerland*
[b] *Institute for Superconducting and Electronic Materials, and ARC Centre of Excellence for Electromaterials Science, University of Wollongong, NSW 2522, Australia*
[c] *Particle Technology Laboratory, Department of Mechanical & Process Engineering, ETH Zürich, CH-8092 Zürich, Switzerland*
[d] *Laboratory of Inorganic Chemistry, ETH Zürich, CH-8093 Zürich, Switzerland*

ARTICLE INFO

Article history:
Received 31 July 2008
Received in revised form 16 December 2008
Accepted 19 December 2008
Available online 30 December 2008

Keywords:
$LiMn_2O_4$
Cathode
Thin film
Flame spray deposition
Lithium-ion battery

ABSTRACT

A new approach has been developed to rapidly synthesize nanostructured $LiMn_2O_4$ thin films by flame spray deposition (FSD) and *in situ* annealing. A precursor solution of lithium acetylacetonate and manganese acetylacetonate in an organic solution was supplied through a flame spray pyrolysis (FSP) reactor. The liquid solution spray was ignited and stabilized by a premixed methane/oxygen flame ring surrounding the FSP nozzle. Thus, $LiMn_2O_4$ nanoparticles were formed by combustion and deposited onto a current collector followed by *in situ* annealing. Two different types of current collectors, i.e. stainless steel and aluminum coated with carbon-based primer were tested. The prepared thin films were characterized by X-ray diffraction and field-emission scanning electron microscopy. The electrochemical properties of the thin films were evaluated by cyclic voltammetry and galvanostatic cycling. The $LiMn_2O_4$ films exhibited good cyclability. Films that underwent sintering and crystal growth during *in situ* annealing developed more robust film structures on the current collector surface and exhibited better electrochemical performance than poorly adhered films.

1. Introduction

Today lithium-ion batteries are the power sources of choice for portable electronics. In the evolving field of portable power systems, lithium-ion (Li-ion) technology seems superior to other battery technologies because of its high working voltage, high energy density, and good cycling stability [1]. Despite its outstanding commercial success, Li-ion battery technology is still open to improvements.

In Li-ion batteries, the most recent candidates as cathode materials are the family of lithium transition metal oxides such as $LiCoO_2$, $Li(Ni,Mn,Co)O_2$, $LiMn_2O_4$, and LiV_3O_8. Among these materials, $LiCoO_2$ is currently used commercially, but is expensive and is not environmentally benign. In comparison, $LiMn_2O_4$ is less toxic and cheaper due to its relative abundance. This spinel oxide is of particular interest for use in hybrid electric vehicles (HEVs) as the cathode material for high-power Li-ion batteries [2,3]. Meanwhile, LiV_3O_8 as a cathode material also has the advantages of higher capacity, lower cost, and better safety features than commercially available $LiCoO_2$ [4,5].

Nevertheless, capacity fading at elevated temperatures and during overcharge has slowed the application of $LiMn_2O_4$ in commercial Li-ion cells. Many studies have been dedicated to the understanding and resolution of the performance degradation. However, precise measurements of the kinetics of Li-ion intercalation under conditions leading to degradation are difficult with powder-based electrodes, since the addition of conductive carbon and binder may influence the electrochemical characterization [6], where degradation often leads to disconnection. Studies of rate processes within powder-based electrodes also suffer from the additional complication of solid-phase and solution-phase resistances [7].

A thin film oxide electrode is a useful model system for the study of electrochemical properties without the above limitations. Advantages of thin film oxide electrodes over powder-based electrodes include: (1) improved understanding of the lithium insertion process and the electrode/electrolyte interface reactions with pure $LiMn_2O_4$, and (2) improved quantification of the effect of morphology [6,8]. Since model electrode materials are fabricated as few micron thick films, they normally add only few ohms to the total internal resistance of the electrochemical cell [9]. Besides, for some applications such as in the industry for miniaturization of electronic devices and for implantation in "smart" credit cards, thin film lithium batteries are also required.

* Corresponding author. Tel.: +41 56 310 2457; fax: +41 56 310 4415.
E-mail address: petr.novak@psi.ch (P. Novák).

0378-7753/$ – see front matter © 2008 Elsevier B.V. All rights reserved.
doi:10.1016/j.jpowsour.2008.12.085

Therefore, thin film fabrication techniques are important in this field.

The preparation of good quality thin films for batteries has been accomplished by chemical vapor deposition [10], pulsed laser deposition [6,11], sputtering [12] and spray pyrolysis [13]. However, most of these methods need expensive apparatuses or are difficult to give the as-deposited thin film accurate stoichiometry. Among them, spray pyrolysis is the most versatile technique for the deposition of active material onto current collectors for its low cost and simplicity. Recently, it has been shown that $LiMn_2O_4$ nanoparticles could be easily prepared by scalable flame spray pyrolysis (FSP) [14] by combustion of appropriate precursor solutions for nanoparticle synthesis with rates up to 1100 g h^{-1} [15]. Furthermore, there are examples in the literature that nanostructured sensing films can be made by FSP and direct deposition of SnO_2 nanoparticles onto sensor substrates [16] and *in situ* annealing [17], leading to stable, transparent, and highly sensitive micro-gas sensors [18]. The opportunity to produce $LiMn_2O_4$ thin films is realized by considering these examples from literature.

Here, flame spray deposition (FSD) and *in situ* annealing [17] are employed to rapidly deposit the $LiMn_2O_4$ nanoparticles onto current collectors to make thin model cathode films. This method does not require the usage of any binder and conductive carbon black. This preparation method has never been applied for the preparation of cathodes in Li-ion batteries. The electrochemical performance of such thin films on different current collectors that were used as model electrodes in Li-ion batteries is investigated.

2. Experimental

2.1. Materials preparation

The FSP method was used to prepare $LiMn_2O_4$ thin films and the experimental setup is described in detail elsewhere [16]. Fig. 1 displays the schematic diagram of that FSP setup. Product $LiMn_2O_4$ particles made by FSP were directly deposited onto the current collector (height above burner, HAB = 150 mm) while the rest were collected on a glass-fiber filter (Whatmann GF/D, 257 mm in diameter). The precursor solution was prepared by dissolving lithium acetylacetonate (Aldrich, purity >97.0%) and manganese (III) acetylacetonate (Aldrich) in a solution, mixture of acetonitrile (Sigma–Aldrich, purity >99.5%) and 2-ethylhexanoic acid (Riedel-de Haën, purity >99%) [14]. The Li:Mn molar ratio was adjusted to 1:2 and the total metal concentration of precursor solution was 0.4 M. The precursor solution was fed into the reactor nozzle (Table 1) by a syringe pump (Inotech R232). The liquid spray was ignited and maintained by a premixed methane/oxygen flame ring surrounding the nozzle exit. The $LiMn_2O_4$ nanoparticles were directly deposited onto stainless steel (SS; Brütsch-Rüegger, Switzerland) and aluminum-coated primer (ACP; GAIA Germany) current collectors. The aluminum-coated primer current collector is a standard aluminum foil coated with a commercial carbon-based primer. The thickness of the aluminum foil is approximately 22 μm and the overall thickness (including the primer) is approximately 24 μm. The SS current collectors were first cleaned with acetone and rinsed with distilled water thrice, whereas the ACP current collectors were used as-received. Both current collectors were mounted on a water-cooled copper block.

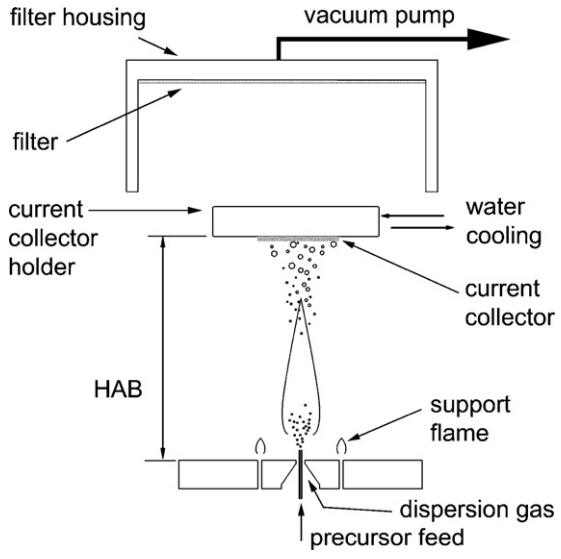

Fig. 1. Schematic of flame spray deposition of $LiMn_2O_4$ onto a water-cooled current collector. Flame-made $LiMn_2O_4$ nanoparticles were directly deposited onto the current collector at a given height above burner (HAB) and the rest were collected on a glass-fiber filter.

Table 1
Growth conditions for $LiMn_2O_4$ thin films.

Current collector	SS and ACP
Precursor solution	$CH_3COCH{=}C(OLi)CH_3$ and $Mn(C_5H_7O_2)_3$ were dissolved in acetonitrile and 2-ethylhexanoic acid [14], total metal concentration 0.4 mol L^{-1}
Premixed CH_4/O_2 flame feed rate	1.13 L min^{-1} CH_4 and 2.40 L min^{-1} O_2
O_2 sheath feed rate	5.00 L min^{-1} O_2
Pressure drop at the nozzle tip	1.5 bar
Syringe pump	5 mL min^{-1}
Current collector temperature	120 °C
Height above burner (HAB)	150 mm
Deposition time	5 min
In situ flame annealing	5 mL min^{-1} of xylene were introduced for 5 min to the FSP unit

The axial temperature profile of a comparable spray flame was measured by Schulz et al. [19] with a maximum of 2400 °C at 50 mm above the burner, decreasing to about 1000 °C at 120 mm above the burner. The precursor used here, however, had 30% less combustion enthalpy density and the current collector was placed 150 mm above burner, so the deposition temperature near the current collector was reduced to less than 500 °C, which is similar to Tricoli et al. [17]. After deposition for 5 min, the deposited film was annealed *in situ* by a pure xylene (Fluka, purity > 97.0%) spray flame. The xylene-FSP flame temperature was estimated to be about 1000 °C above the burner [17]. However, the temperature of the current collector was reduced to approximately 120 °C as it was attached to the water-cooled copper block during the entire deposition and annealing process. The temperature was measured at the back side of the current collector [16]. The growth or synthesis conditions of $LiMn_2O_4$ thin films are shown in detail in Table 1.

2.2. Materials characterization

The Brunauer–Emmett–Teller (BET) specific surface area, S_{BET}, of the powder before and after *in situ* annealing, collected from the glass fiber was determined by five-point nitrogen adsorption isotherm at 77 K, using the Micromeritics Tristar 3000. All samples were degassed in N_2 at 150 °C for 1 h prior to analysis. X-ray diffraction (XRD) patterns of the thin film samples on the current collectors were measured using a Bruker AXS D8 Advance device operated at 40 kV, 40 mA with Cu Kα radiation (λ = 1.5405 Å) and analyzed with a TOPAS 2 software. The surface morphology of the $LiMn_2O_4$ thin film was observed by field-emission scanning electron microscopy (FE-SEM, LEO 1530 Gemini) operated at 1 kV.

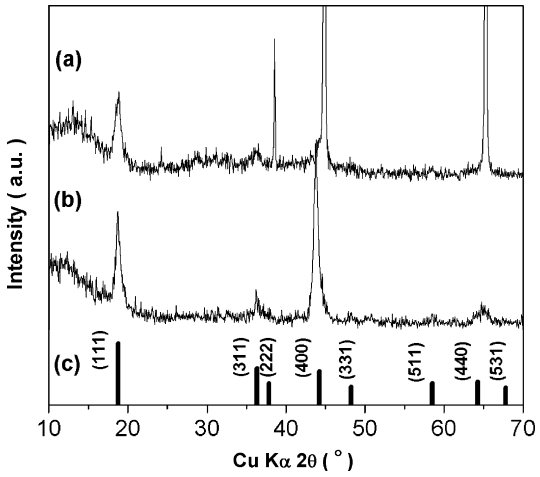

Fig. 2. XRD spectra of *in situ* annealed $LiMn_2O_4$ films on (a) aluminum-coated primer (ACP) and (b) stainless steel (SS) current collectors; and (c) standard $LiMn_2O_4$ powder from JCPDS Card No. 35-0782.

2.3. Electrochemical characterization

The $LiMn_2O_4$ nanoparticle films on the current collector were cut into 1.0 cm^2 squares with the active material loading of about 0.05 mg cm^{-2}. It was then dried at 120 °C in vacuum for 12 h and used as electrodes directly. Electrochemical test cells similar to coin-type cells [20] were assembled using the $LiMn_2O_4$ thin films as the working electrode and the Li metal (Aldrich, 99.9%) as both the counter and reference electrode. Both electrodes were separated by a 1-mm thick glass-fiber separator saturated with 500 μL of electrolyte solution. The electrolyte solution used was 1 M $LiPF_6$ in ethylene carbonate (EC):dimethyl carbonate (DMC), 1:1 in mass ratio (Ferro Corp., USA). The cells were assembled in an argon-filled glove box with less than 1 ppm of oxygen, nitrogen, and water contents.

Cyclic voltammetry (CV) and galvanostatic charge and discharge measurements were performed by a computer-controlled cell-data capture (CCCC) system (Astrol Electronic AG, Oberrohrdorf, Switzerland). The CV measurements were performed in the range of 3.50–4.30 V vs. Li/Li^+ at scanning rate of 0.02 mV s^{-1}. Other cells were galvanostatically charged and discharged in the same potential range at a constant specific current of 40 mA g^{-1}. In order to promote complete charge–discharge at the respective potential limits, a potentiostatic step was included until the specific current was 10% of the current used in the galvanostatic step.

3. Results and discussion

3.1. Characterization of the materials

The crystallinity and purity of the thin films before and after *in situ* flame annealing was determined by XRD. Fig. 2 shows the XRD diffractograms of such films after annealing on SS and ACP collectors. These patterns are consistent with conventionally and FSP-made $LiMn_2O_4$ nanoparticles [14]. They appeared to be in good agreement with the known spinel phases (Fig. 2c) with a space group *Fd*3*m* given in the literature (JCPDS 35-0782). Two major peaks corresponding to (1 1 1) and (3 1 1) planes of spinel $LiMn_2O_4$ were clearly observed. The (4 0 0) peak at 44.1° for both thin film samples overlapped with the peak of the applied current collector. There is no notable intensity variation induced by a secondary phase or any impurities for both samples after *in situ* annealing. The XRD crystal size was about 10 nm for the material on both current collectors before annealing. After annealing the films on the ACP current collector, no discernible change was observed in XRD crystal size. In contrast, the XRD crystal size of the films on the SS current collector increased by 30% to 13 nm by *in situ* flame annealing indicating significant crystal growth by sintering.

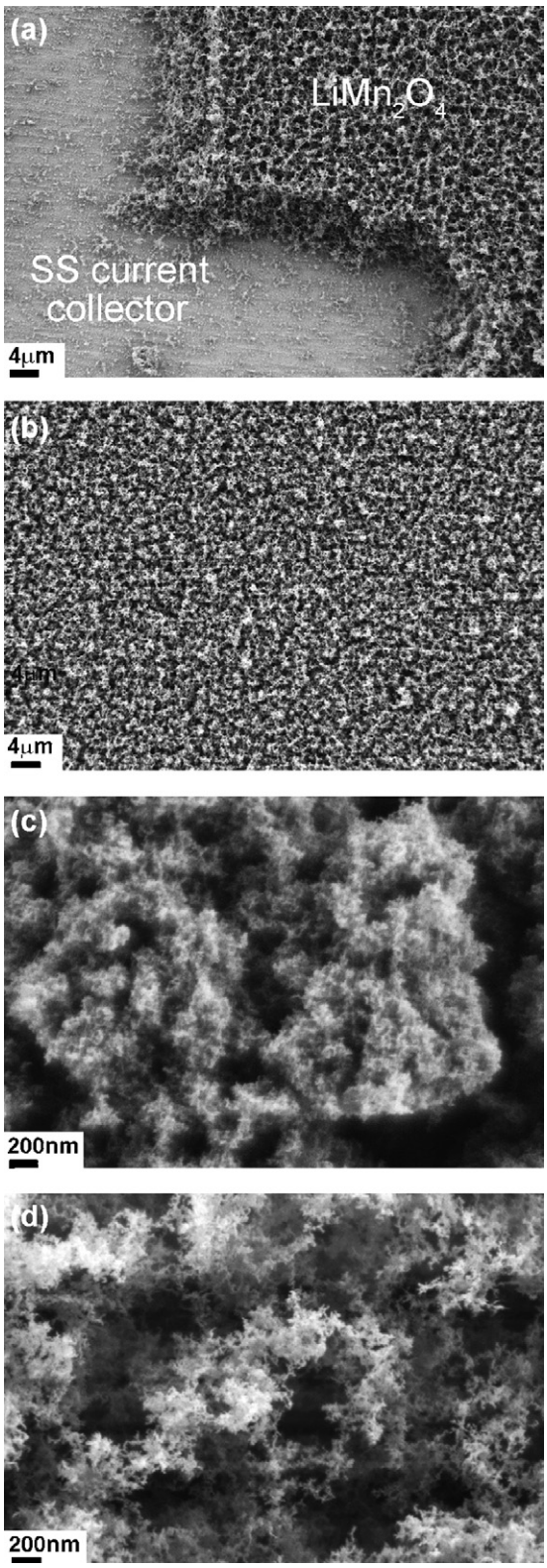

Fig. 3. The morphology of FSP-made $LiMn_2O_4$ nanoparticles as-deposited onto (a) SS and (b) ACP current collectors; and after *in situ* annealing onto the (c) SS and (d) ACP current collectors.

Fig. 3 shows the morphology of these $LiMn_2O_4$ films before and after *in situ* flame annealing onto SS and ACP current collectors as determined by FE-SEM. Fig. 3a shows the surface of the thin film after direct deposition for 5 min on a SS current collector without *in situ* annealing. It is clear that a homogeneous film with a thickness of ~7 μm was formed. This film is highly porous (98% porosity is expected [16]) with a lace-like structure of uniformly sized nanograins similar to SnO_2 sensor film deposited by this method [16,17]. The corresponding films on the ACP current collector have similar morphology (Fig. 3b). Essentially, there are no detectable cracks or variation in film structure as no solvent evaporation takes place by this technique in contrast to wet-deposition of slurries or pastes [16]. When these films undergo *in situ* annealing on the SS current collector (Fig. 3c), most of the nanoparticles are rather densely packed together forming cauliflower-like structures [17]. This is quite different than the corresponding ACP films (Fig. 3d) that have remained virtually unchanged by that annealing. It should be noted that the ACP current collector (with the carbon-based primer coated onto the aluminum foil) is not stable after *in situ* annealing. The adhesion between the nanoparticles and the ACP surface is poorer than that of SS as has also been observed for sensor micropatterning of lace-like film structures [17]. These results are consistent with the above XRD crystal size data that indicated crystal growth by sintering took place in the SS collector by *in situ* annealing in contrast to ACP current collector. Consistent with the above trend though not directly comparable because of the difference in high temperature residence time distribution with the particles deposited on current collectors, the S_{BET} of nanoparticles collected on the filter paper is approximately 134 $m^2\ g^{-1}$ before annealing while after annealing is reduced to about 124 $m^2\ g^{-1}$.

3.2. Electrochemical performance

The as-synthesized $LiMn_2O_4$ thin films (grown without the *in situ* annealing FSD, for both SS and ACP current collectors) have no obvious redox peaks (not shown here) and thus the *in situ* annealing was applied to improve the crystallinity of the thin films and to enhance their conductivity and/or the contact to the current collector. A slow scan CV for the $LiMn_2O_4$ thin films after *in situ* annealing is shown in Fig. 4 for the initial cycle. According to Fig. 4, the *in situ* annealed $LiMn_2O_4$ thin films are electrochemically active in the applied potential range. Two pairs of redox peaks at approximately 4.00 and 4.15 V vs. Li/Li^+ are clearly observed, indicating two stages of the Li-ions extraction and insertion [2,3]. This is a typical characteristic of the Li^+ intercalation/de-intercalation process of the $LiMn_2O_4$ spinel during the electrochemical reaction [2]. The redox peaks for both *in situ* annealed $LiMn_2O_4$ thin films are sharp with well-defined splitting. In particular, the peaks for the thin film grown on the SS current collector are more symmetric with narrower peaks, thus suggesting better suitability of films on SS current collectors for model electrochemical experiments.

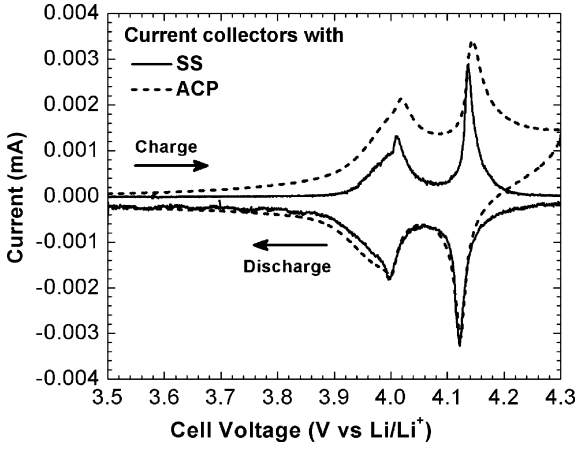

Fig. 4. Cyclic voltammograms of *in situ* annealed $LiMn_2O_4$ thin film electrodes on SS and ACP current collectors at scan rates of 0.02 mV s^{-1} for the initial cycle.

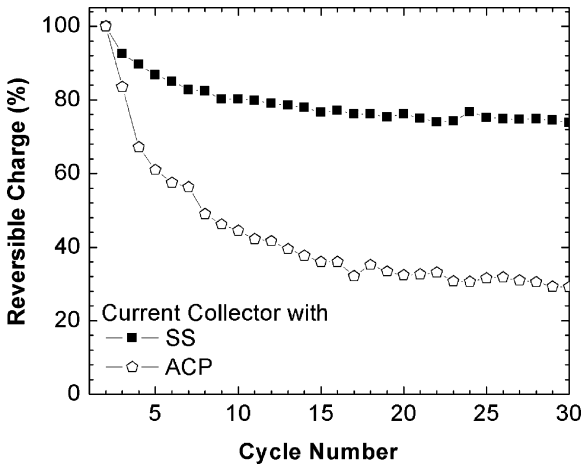

Fig. 5. Reversible charge as a function of cycle number from the galvanostatic experiments of the *in situ* annealed $LiMn_2O_4$ thin film electrodes on the SS and ACP current collectors.

Fig. 5 shows the reversible charge of the electrodes prepared with the *in situ* annealing $LiMn_2O_4$ nanoparticles deposited onto the SS and ACP current collector upon cycling. Capacity fading is observed after several charge/discharge cycles in all cases, but the decay of the charge capacity for *in situ* annealed $LiMn_2O_4$ nanoparticles deposited on the SS current collector is much slower than those on the ACP current collector. The former electrode has in average only 0.87% charge loss per cycle in 30 cycles. The ratio for the charge respective to the two peaks of film grown onto the SS current collector is close to unity (cf. Fig. 4), and therefore it confirms the better reversibility of the cell. The improved performance of the SS collector is attributed to the better adhesion of the cauliflower-like $LiMn_2O_4$ thin films on its surface.

The results in Figs. 4 and 5 indicate that the electrochemical response of the prepared $LiMn_2O_4$ thin films depends on the dynamics of particle or crystal growth, adhesion, and type of current collector. The mechanical properties of these cathode films are still poor due to the porous and fractal-like surface morphology [17,21]. According to Fragnaud et al. [13], the current collector temperature during spray pyrolysis substantially modifies the morphology and adhesion of the films. Hence, further improvement will be focused on the preparation of dense and tough layer of $LiMn_2O_4$ thin films with good adhesion properties to the SS current collector.

4. Conclusions

The present studies indicate that spinel $LiMn_2O_4$ thin films can be prepared by a novel method, flame spray deposition and *in situ* annealing. This simple, fast, and efficient method has never been applied for the preparation of cathode materials. Two pairs of electrochemically active redox peaks are clearly observed. This indicates that the prepared electroactive $LiMn_2O_4$ thin films made without any binder and conductive carbon black could be used as model electrodes to study the electrochemical behavior in lithium-ion batteries. In particular, nanostructured thin films that have adhered better by sintering and crystal growth on current collectors seem to perform better electrochemically than thin films which were not sintered.

Acknowledgments

Financial support from the Australian Research Council through the ARC Centre of Excellence Grant CE0561616 (S.Y. Chew, J.Z. Wang, and H.K. Liu), CCMX, Nanoprim (A. Tricoli), and ETH Research Grant TH-09/06-2 (R. Büchel) are gratefully acknowledged. Special thanks to EMEZ, ETH Zürich for the electron microscopic measurement. Technical assistance from Mr. W. Scheifele (PSI) and Mr. H. Kaiser (PSI) is highly appreciated.

References

[1] J.-M. Tarascon, M. Armand, Nature 414 (2001) 359–367.
[2] M. Winter, J.O. Besenhard, M.E. Spahr, P. Novák, Adv. Mater. 10 (1998) 725–763.
[3] J.M. Tarascon, D. Guyomard, Electrochim. Acta 38 (1993) 1221–1231.
[4] A.M. Kannan, A. Manthiram, J. Power Sources 159 (2006) 1405–1408.
[5] S.Y. Chew, C. Feng, S.H. Ng, J. Wang, Z. Guo, H. Liu, J. Electrochem. Soc. 154 (2007) A633–A637.
[6] F. Simmen, T. Lippert, P. Novák, B. Neuenschwander, M. Döbeli, M. Mallepell, A. Wokaun, Appl. Phys. A 93 (2008) 711–716.
[7] C.H. Chen, E.M. Kelder, J. Schoonman, J. Power Sources 68 (1997) 377–1194.
[8] K.A. Striebel, A. Rougier, C.R. Horne, R.P. Reade, E.J. Cairns, J. Electrochem. Soc. 146 (1999) 4339–4347.
[9] M.P. Vinod, D. Bahnemann, J. Solid State Electrochem. 6 (2002) 498–501.
[10] K.W. Kim, M.R. Kim, S.W. Lee, K.S. Han, S.I. Woo, Chem. Vapor Depos. 9 (2003) 187–192.
[11] D. Singh, R. Houriet, R. Giovannini, H. Hofmann, V. Craciun, R.K. Singh, J. Power Sources 97 (2001) 826–831.
[12] J. Xie, T. Tanaka, N. Imanishi, T. Matsumura, A. Hirano, Y. Takeda, O. Yamamoto, J. Power Sources 180 (2008) 576–581.
[13] P. Fragnaud, R. Nagarajan, D.M. Schleich, D. Vujic, J. Power Sources 54 (1995) 362–366.
[14] F.O. Ernst, H.K. Kammler, A. Roessler, S.E. Pratsinis, W.J. Stark, J. Ufheil, P. Novák, Mater. Chem. Phys. 101 (2007) 372–378.
[15] R. Mueller, L. Madler, S.E. Pratsinis, Chem. Eng. Sci. 58 (2003) 1969–1976.
[16] L. Mädler, A. Roessler, S.E. Pratsinis, T. Sahmb, A. Gurlo, N. Barsan, U. Weimar, Sens. Actuator B Chem. 114 (2006) 283–295.
[17] A. Tricoli, M. Graf, F. Mayer, S. Kühne, A. Hierlemann, S.E. Pratsinis, Adv. Mater. 20 (2008) 3005–3010.
[18] S. Kühne, M. Graf, A. Tricoli, F. Mayer, S.E. Pratsinis, A. Hierlemann, J. Micromech. Microeng. 18 (2008), 035040 (10 pp.).
[19] H. Schulz, L. Madler, R. Strobel, R. Jossen, S.E. Pratsinis, T. Johannessen, J. Mater. Res. 20 (2005) 2568–2577.
[20] P. Novák, W. Scheifele, F. Joho, O. Haas, J. Electrochem. Soc. 142 (1995) 2544–2550.
[21] C.H. Chen, J. Schoonman, J. Ind. Eng. Chem. 10 (2004) 1114–1125.